7.3. Thermal neutron detection

BY P. CONVERT AND P. CHIEUX

7.3.1. Introduction

In this chapter, we shall be concerned with the detection of neutrons having thermal and epithermal energies in the range 0.0002–10 eV (20–0.1 Å). Given the cost and the rarity of the neutron sources, it is clear that the recent trends in neutron diffractometry are more and more in the direction of designing new instruments around highly efficient and complex detection systems. These detection systems become more and more adapted to the particular requirements of the different experimental needs (counting rate, size, resolution, definition, shielding and background, TOF, *etc*.). It is therefore difficult to speak about neutron detectors and intensity measurements as such without reference to the complete spectrometers, and this should include the on-line computer.

Most neutron detectors for research experiments have been created and developed using fission reactors as neutron sources [*i.e.* with an upper limit of usable energy of 0.5 eV (0.4 Å)]. Given the relatively low intensity of reactor neutron beams, a very successful effort has been made to increase the detector efficiency and the detection area as much as possible. The recent construction of pulsed neutron sources extends the range of incident energy to at least 10 eV and generalizes the use of time-of-flight (TOF) techniques. A broad range of fully operational neutron detectors, well adapted to reactors as neutron sources, is commercially available, but this is not yet the case for pulsed sources. Probably due to the variation of intensity of the early neutron beams, it is a tradition in neutron research to monitor the incident flux with a low-efficiency detector, which in the best case has a stability of the order of 10^{-3}, *i.e.* sufficient for most experiments.

7.3.2. Neutron capture

Neutrons' lack of charge and the fact that they are only weakly absorbed by most materials require specific nuclear reactions to capture them and convert them into detectable secondary particles. Table 7.3.2.1 lists the neutron-capture reactions that are commonly used in thermal neutron detection. The incoming thermal neutron brings a negligible energy to the nuclear reaction, and the secondary charged particles or fission fragments are emitted in random directions following the conservation-of-momentum law $\sum m_i v_i = 0$. The capture or absorption cross sections for a number of nuclei of interest are plotted as a function of neutron energy in Fig. 7.3.2.1. These cross sections are commonly expressed in barns (1 barn = 10^{-28} m^2). At low energies, they are inversely proportional to neutron velocity, except in the case of Gd, which has a nuclear resonance at 0.031 eV. The total efficiency ε of neutron detection can be expressed by the equation

$$\varepsilon = \xi[1 - \exp(-N\sigma_a t)], \qquad (7.3.2.1)$$

where N is the number of absorbing nuclei per unit volume, σ_a is their energy-dependent absorption cross section, and t is the thickness of the absorbing material. The factor $1 - \exp(-N\sigma_a t)$ gives the neutron-capture efficiency, while ξ is a factor ≤ 1 that depends on the detector geometry and materials (absorption and scattering in the front window) and on the efficiency of the secondary particles.

7.3.3. Neutron detection processes

A detection process consists of a chain of events that begins with the neutron capture and ends with the macroscopic 'visualization' of the neutron by a sensor (electronic or film). The quality of a detection process will depend on the efficiency of the conversion steps and on the characteristics of the emission steps, which alternate in the process (see Table 7.3.3.1). We present below typical detection processes.

7.3.3.1. *Detection via gas converter and gas ionization: the gas detector*

The neutron capture and the trajectories of the secondary charged particles as well as the specific gas ionization along these trajectories are presented in Figs. 7.3.3.1(*a*) and (*b*). Since the gas ionization energy is about 30 eV per electron (42 eV for ^{3}He and 30 eV for CH_4), there are about 25 000 ion pairs (e^-, He^+ or e^-, CH_4^+) per captured neutron. Gases such as CH_4 or C_3H_8 are added to diminish the length of the trajectories, *i.e.* the wall effect [see Subsection 7.3.4.2(*b*)].

We give in Fig. 7.3.3.1(*c*) the proton range of an ^{3}He neutron-capture reaction in various gases (Fischer, Radeka, & Boie, 1983). A schematic drawing of a gas monodetector, which might be mounted either in axial or in radial orientation in the neutron beam, is given in Fig. 7.3.3.1(*d*).

For this type of detector, the efficiency as a function of the gas pressure, or gas-detector law, is written as

$$\varepsilon(\lambda) = \xi[1 - \exp(-bPt\lambda)],$$

with P (atm) = the detector-gas pressure at 293 K, t (cm) = the gas thickness, and λ (Å) = the detected neutron wavelength. The numerical coefficient b, obtained at 293 K from the ideal gas law, the Avogadro number N_A, and the gas absorption cross section σ_a (barns) at $\lambda_0 = 1.8$ Å, is

$$b = \frac{273}{293} \times \frac{N_A}{22\,414} \times \frac{\sigma_a}{\lambda_0}.$$

For ^{3}He, with $\sigma_a = 5333$ barns at $\lambda_0 = 1.8$ Å, $b = 0.07417$; for $^{10}BF_3$, with $\sigma_a = 3837$ barns at $\lambda_0 = 1.8$ Å, $b = 0.0533$. We give in Table 7.3.3.2 a few examples of gas-detector characteristics.

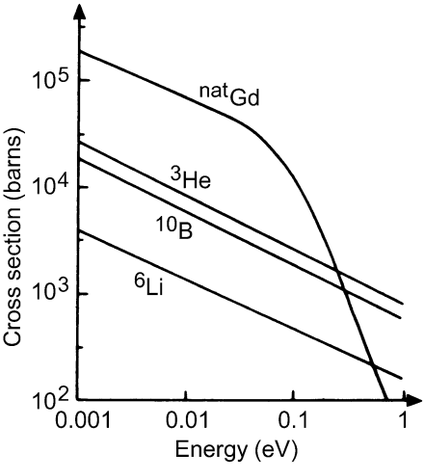

Fig. 7.3.2.1. The capture cross sections for a number of nuclei used in neutron detection. [Adapted from Convert & Forsyth (1983).]

Copyright © 2006 International Union of Crystallography

Table 7.3.2.1. *Neutron capture reactions used in neutron detection*

n = neutron, p = H^+ = proton, t = $^3H^-$ = triton, $\alpha = {}^4H^+$ = alpha, e^- = electron

Capture reaction	Cross section at 1 Å (barns)	Secondary-particle energies (MeV)
$^3He + n \rightarrow t + p$	3000	t 0.20 p 0.57
$^6Li + n \rightarrow t + \alpha$	520	t 3.74 α 2.05
$^{10}B + n \rightarrow {}^7Li^* + \alpha$ (93%) $\hookrightarrow {}^7Li + \gamma$ $\rightarrow {}^7Li + \alpha$ (7%)	2100	α 1.47 ^7Li 0.83 γ 0.48 α 1.78 ^7Li 1.01
$^{157}Gd + n \rightarrow Gd^*$ $\hookrightarrow \gamma$ + conversion electrons	74000 (^{nat}Gd: 17000)	e^- spectrum 0.07 to 0.182 γ spectrum up to 8
$^{235}U + n \rightarrow$ fission fragments	320	Fission fragments up to 80

There are two modes of operation.

In the case of *direct collection of charges*, the 25 000 electrons corresponding to one neutron capture (*primary electrons*) are collected by the anode in about 100–500 ns, and generate an input pulse in the charge preamplifier (see Section 7.3.4).

If the electrical field created by the high voltage applied to the anode exceeds a critical value, the electrons will be accelerated sufficiently to produce a cascade of ionizing collisions with the neutral molecules they encounter, the new electrons liberated in the process being called *secondary electrons*. This phenomenon, *gas multiplication*, occurs in the vicinity of the thin wire anode, since the field varies as $1/r$. The avalanche stops when all the free electrons have been collected at the anode. With proper design, the number of secondary electrons is proportional to the number of primary electrons. For cylindrical geometries, the multiplication coefficient M can be calculated (Wolf, 1974). This type of detection mode is called the proportional mode. It is very commonly used because it gives a better signal-to-noise ratio (see Section 7.3.4).

A few critical remarks about gas detectors:

(i) Some gases have a tendency to form negative ions by the attachment of a free electron to a neutral gas molecule, giving a loss of detector current. This effect is negligible for ^3He but it limits the use of $^{10}BF_3$ to about 2 atmospheres pressure, although traces of gases such as O_2 or H_2O (*e.g.* detector materials and wall outgasing) are often the reason for loss by attachment.

(ii) Pure ^3He and $^{10}BF_3$ gas detectors are practically insensitive to γ radiation. This is no longer the case when additional gases, which are necessary for ^3He, are used, although the polyatomic additives C_3H_8 and CF_4 are much better than the rare gases Kr, Xe, and Ar (Fischer, Radeka & Boie, 1983).

(iii) For various reasons (the price of ^3He and $^{10}BF_3$ and the toxicity of BF_3), neutron gas detectors are closed chambers, which must be leak-proof and insensitive to BF_3 corrosion. The wall thickness must be adapted to the inside pressure, which sometimes implies a rather thick front aluminium window (*e.g.* a 10 mm window for a 16 bar ^3He gas position-sensitive detector; aluminium is chosen for its very good transmission of neutrons, about 90% for 10 mm thickness).

7.3.3.2. *Detection via solid converter and gas ionization: the foil detector*

This mode of detection is generally used for monitors. In a typical design, a ^{10}B deposit of controlled thickness, for example $t = 0.04\,\mu m$ giving a capture efficiency of 10^{-3} at $\lambda = 1$ Å, is made on a thin aluminium plate (see Fig. 7.3.3.2). One of the two particles (α, Li) produced in the solid by the capture reaction is absorbed by the plate; the other escapes and ionizes the gas. The electrons produced are collected by the aluminium plate, itself acting as the anode, or by a separate anode wire, allowing the use of the proportional mode. The detection efficiency is proportional to the deposit thickness t, but t must be kept less than the average range r of the secondary particles in the deposit (for ^{10}B, $r_\alpha = 3.8\,\mu m$ and $r_{Li} = 1.7\,\mu m$), which limits the efficiency to a maximum value of 3–4% for $\lambda = 1$ Å. The fraction of the secondary particle energy that is lost in the deposit reduces the detector current, *i.e.* the signal-to-noise ratio, and worsens the amplitude spectrum (see Section 7.3.4).

7.3.3.3. *Detection via scintillation*

In the detection process *via* scintillation (see Table 7.3.3.1), the secondary particles produced by the neutron capture ionize and excite a number of valence-band electrons of the solid scintillator to high-energy states, from which they tend to decay with the emission of a light flash of photons detected by a photomultiplier [see Fig. 7.3.3.3(*a*)]. A number of conditions must be satisfied:

(i) The scintillation must be immediate after the neutron-capture triggering event.

(ii) The scintillation decay time must be short. It depends on materials, and is around 50–100 ns for lithium silicate glasses.

(iii) A large fraction of the energy must be converted into light (rather than heat).

(iv) The material must be transparent to its own radiation.

Most thermal neutron scintillation detectors are currently based on inorganic salt crystals or glasses doped with traces of an activating element (Eu, Ce, Ag, *etc.*) (extrinsic scintillators). (A plastic scintillator might be considered to be a solid organic solution with a neutron converter.)

The use of extrinsic scintillators (Convert & Forsyth, 1983), although less efficient energetically, permits better decoupling of the energy of the photon-emitting transition (occurring now in the activator centres) from that of the valence-band electron excitation or ionization energy. The crystal or glass is then transparent to its own emission, and the light emitted is shifted to a wavelength better adapted to the following optical treatment.

Table 7.3.3.1. *Commonly used detection processes*

	1st conversion (neutron captures)	2nd conversion	3rd conversion	Sensor
	Capture/solid $\rightarrow e^-$ $n + {}^{157}Gd$			Film
Gas ionization	Capture/gas $n + {}^3He \rightarrow p + t$	Gas ionization $\rightarrow e^-$ (^3He + add. gas)		Electronics
	Capture/solid $n + {}^{10}B, {}^6Li, {}^{235}U$ fission products	Gas ionization $\rightarrow e^-$ (*e.g.* Ar + CO_2)		Electronics
Scintillation	Capture/solid:	Fluorescence/solid:		
	LiF + ZnS(Ag) $n + {}^6Li \rightarrow \alpha + t$	LiF + ZnS(Ag) $\rightarrow \nu$		Film
	LiF + ZnS(Ag) $n + {}^6Li \rightarrow \alpha + t$	LiF + ZnS(Ag) $\rightarrow \nu$	Photoelectric effect $\rightarrow e^-$	Electronics
	Ce^{3+} enriched Li glass $n + {}^6Li \rightarrow \alpha + t$	Ce^{3+} enriched Li glass $\rightarrow \nu$	Photoelectric effect $\rightarrow e^-$	Electronics

ν = photon.

Table 7.3.3.2. *A few examples of gas-detector characteristics*

Detection gas	Additional gas	Gas pressure (atm)	Useful detection volume (mm × mm)	Mounting	Capture efficiency	
					$\lambda = 1$ Å	$\lambda = 2$ Å
$^{10}BF_3$		1	$L = 200$, Ø = 50	Axial Radial*	65.5% 23.4%	88.1% 41.3%
^3He		5	$L = 100$, Ø = 50	Axial Radial*	97.5% 84.4%	99.9% 97.5%
^3He		8	$L = 250$, Ø = 10	Radial*	44.7%	69.5%
^3He (monitor)	C_3H_8	2	100 × 40 × 40		10^{-5} to 10^{-3}	

* Value calculated for the diameter.

In order to maximize the light collected by the photomultiplier [Fig. 7.3.3.3(*b*)], a light reflector is added in front of the scintillator, and a light coupler adapts the dimensions of the scintillator to that of the photomultiplier (PM). The area of the scintillator might be very large (up to 1 m^2). The optimum thickness of a glass scintillator is about 1 to 2 mm, corresponding to a neutron detection efficiency of 40 to 97% for $\lambda = 1.8$ Å, depending on the ^6Li concentration (Strauss, Brenner, Chou, Schultz & Roche, 1983). In a Ce-doped Li silicate glass, the number of photons emitted per captured neutron is about 9000, giving finally about 1500 electrons at the photocathode in the optimum light-coupling configuration. The number of photons emitted per captured neutron, the number of those reaching the photocathode, and the scintillator decay time are parameters that might differ by an order of magnitude, depending on the scintillator material. However, the glass scintillator remains for the time being the best choice, since the possible gains given by other materials, in decay time or in the number of photons emitted, are always very severely offset by poor light output (*e.g.* the plastic scintillator). It is very important to maximize the number of photons per neutron reaching the photocathode, since this will help to discriminate between neutrons and γ rays [see Fig. 7.3.4.2(*e*)]. The optical coupling between the different parts of the detection system must be of very good quality.

7.3.3.4. *Films*

Films are classed as position-sensitive detectors. Two types of neutron converter are used in neutron film-detection processes. In the case of the scintillation film system, a light-sensitive film is pressed close to one or between two plastic $^6LiF/ZnS(Ag)$ scintillator screens (Thomas, 1972). In the case of the Gd-foil

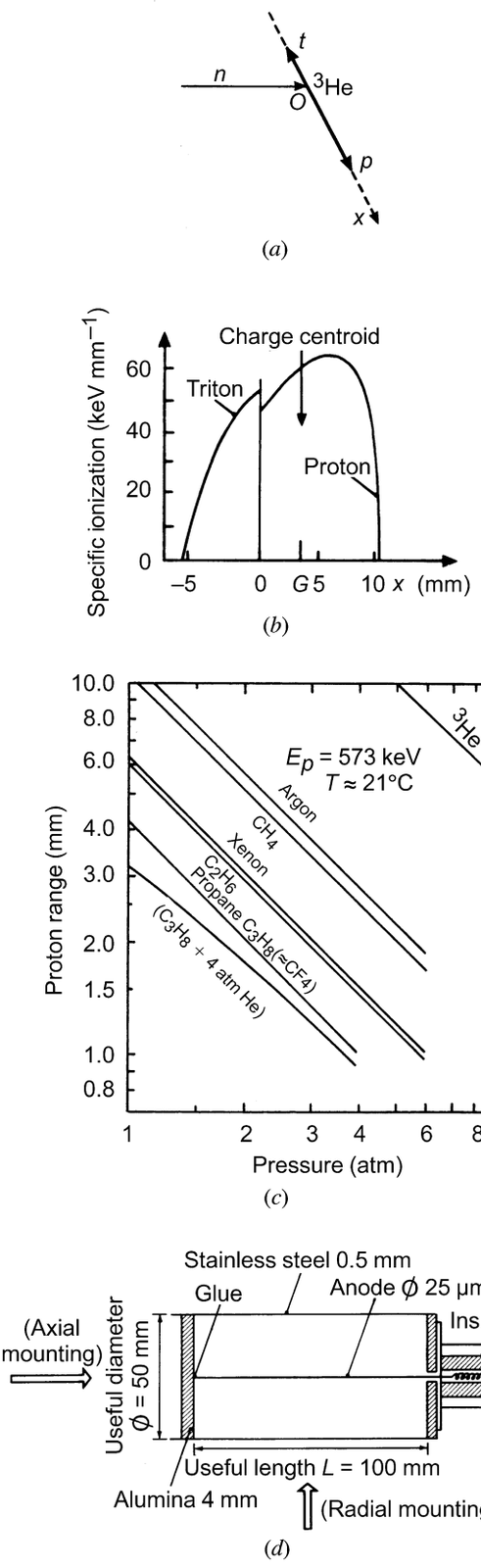

Fig. 7.3.3.1. (*a*) Neutron capture by an ^{3}He atom and random-direction trajectory (*Ox*) of the secondary charged particles in the gas mixture. (*b*) Calculated specific ionization along the proton and triton trajectory in a 65% ^{3}He/35% CH_4 mixture at 300 K and atmospheric pressure (Whaling, 1958). [Reproduced from Convert & Forsyth (1983).] (*c*) Range of a 0.57 MeV proton (from ^{3}He neutron capture) as a function of the pressure of various gases. [Reproduced from Convert & Forsyth (1983).] (*d*) Schematic drawing of a gas monodetector. The arrows represent the incoming beam.

converter, the conversion electrons are emitted isotropically, with a main energy peak at 72 keV, and collected by an X-ray film in close contact with the converter (Baruchel, Malgrange & Schlenker, 1983).

In addition to the advantages given by the film technique in itself (simplicity, low price, direct picture, *etc.*), neutron photographic methods give the best spatial resolution. However, the resolution is inversely related to the detector efficiency and thickness. A good compromise appears to be a thickness of 0.25 mm for a plastic scintillator [*i.e.* a capture efficiency of about 12% and a resolution of 0.1 mm for a one-screen converter at $\lambda = 1$ Å; see the size of the ionization volumes in a scintillator, Fig. 7.3.3.3(*a*)]. Here, however, as in light scattering, the optical density depends on the exposure time as well as on the incoming flux (Schwartzschild effect), which necessitates a calibration (Hohlwein, 1983). For a natural Gd-foil converter, an optimum thickness is 0.025 mm, giving a resolution of 0.020 mm. The Gd-foil film detector is one order of magnitude

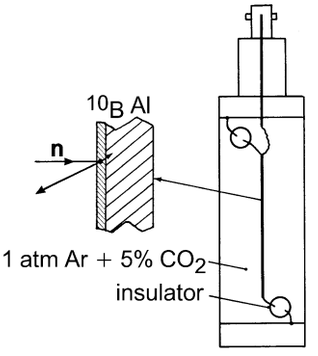

Fig. 7.3.3.2. Typical design of a ^{10}B-foil detector.

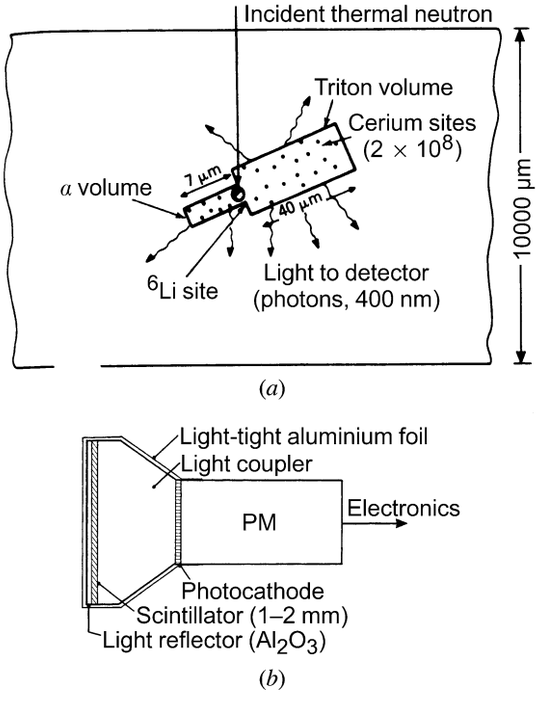

Fig. 7.3.3.3. (*a*) Schematic representation of the neutron capture, secondary α, and triton ionization volumes, and scintillator light emission in a cerium-doped lithium silicate glass. [Reproduced from Convert & Forsyth (1983).] (*b*) Schematic representation of a scintillation detector.

less efficient than the scintillator, but, as in electron microscopy, the optical density is nearly proportional to the exposure. This explains the use of the Gd foil in neutron-diffraction topography.

If we take into account the possible inhomogeneity of the converter and the difficulties related to the film (homogeneity, development, and photodensitometry), an accuracy of 5 to 10% is achievable in the intensity measurements under good conditions.

Owing to the differences in the processes, neutron photographic techniques are much more efficient than those for X-rays. In the case of the plastic scintillator, the gain is about 10^3, which compensates for the much lower neutron fluxes.

7.3.4. Electronic aspects of neutron detection

7.3.4.1. *The electronic chain*

Each collected burst of electrons, corresponding to one captured neutron, will be successively amplified, identified (discriminated), and transformed to a well defined signal, by a chain of electronic devices that are represented in Fig. 7.3.4.1. In the case of the gas detector, the complete electronic chain is generally contained in a grounded metallic box acting as an electrical shield. The detector is connected to this box *via* a coaxial cable as short as possible to avoid noise and parasitic capacitance. A high-voltage power supply feeds the detector anode through a filter. The charge-sensitive preamplifier contains a field-effect transistor (FET) to minimize the background noise, since, from the detector up to this stage, the electronic level is very low. At the output of the FET, the pulse corresponding to one neutron has an amplitude of about 20 mV. This pulse enters an operational amplifier with adjustable gain G, which delivers a signal of about 2 V, the analogue signal (ANA). The electronic pulse-rise time (0.5 to a few μs) is adapted to the detector electron-collecting time, *i.e.* its amplitude is roughly proportional to the number of electrons collected at the anode. The last part of the electronic chain is a discriminator with an adjustable threshold, followed by a trigger delivering a calibrated signal (*e.g.* +5/0 V), called the logic signal (LOG), which is sent to a scaler.

In the case of the scintillator, the photomultiplier ensures the conversion of light to electrons and produces a strongly amplified electronic signal that is processed through a discriminator and trigger as for the gas detector.

7.3.4.2. *Controls and adjustments of the electronics*

For the gas detector, there are basically three parameters to be adjusted, the gas-amplification coefficient M (a function of the detector high voltage), the electronic amplification gain G, and the discriminator threshold T. Since these adjustments are interactive, the high voltage is initially set at the value given by the manufacturer. The gain G is adjusted in order not to saturate the amplifier. When the electronic amplifier power supply voltage is 5 V, a typical setting of the pulse maximum amplitudes is about 3 V.

We present now the three types of operation necessary to adjust the electronics.

(*a*) *Control of the pulse shape*. The analogue pulse ANA (see Fig. 7.3.4.1) is directly observed with an oscilloscope. Depending on the construction of the electronic chain, it is important to verify if the input of the oscilloscope (or of the multichannel analyser, see below) must be adapted with a 50 Ω impedance or not. This will ensure that the amplitude of the analogue pulse and the accessible value of the voltage threshold are on the same scale (and not different by a factor of two). Fig. 7.3.4.2(*a*) shows characteristic shapes obtained when triggering the oscilloscope at, say, 0.2 V and observing a $^{10}BF_3$ gas detector either pulse by pulse or in a continuous way. This type of display allows the trained user to check the noise level, the amplitudes of the neutron pulses, the quality of the pulse shape, and the presence of any anomalous signal such as one due to flashes of parasitic electronic or electric noise (*e.g.* 50 Hz). γ rays produce fewer electrons than neutrons, so that the corresponding pulses are of a lower amplitude (by a factor of 1/5 to 1/20).

(*b*) *Control of the distribution of the pulse amplitudes*. The distribution of amplitudes of the various pulses in number of pulses per amplitude increment dN/dA is analysed and displayed using a multichannel analyser. Fig. 7.3.4.2(*b*) shows the amplitude spectrum for a $^{10}BF_3$ gas detector. The main peak at A_0 corresponds to the main neutron-capture reaction (2.3 MeV, 93%). From its FWHM, we define the detector electronic resolution $\Delta A/A_0$. The right-hand-side small peak is due to the 2.8 MeV, 7% capture reaction. The tail of amplitudes down to $4A_0/11$ corresponds to neutrons captured near the detector walls, which stop some of the secondary-particle trajectories (wall effect). The existence of a deep valley [see Fig. 7.3.4.2(*b*)] where the discriminator threshold T is placed ensures that all captured neutrons, and nothing else, are counted. The width of this valley guarantees good detection stability. Three effects might reduce this valley. Worsening of the gas quality will reduce all the pulse amplitudes (neutron and gamma), an increase in electronic noise will result in a resolution loss affecting the valley on both sides, and a high level of γ radiation will produce a pile up of the independent γ pulses, increasing their amplitude.

(*c*) *Optimization of the threshold and high-voltage values*. In order to set the threshold T at its optimum value for discrimination and stability, the total number of counts in the detector per unit time is plotted as a function of the threshold, for

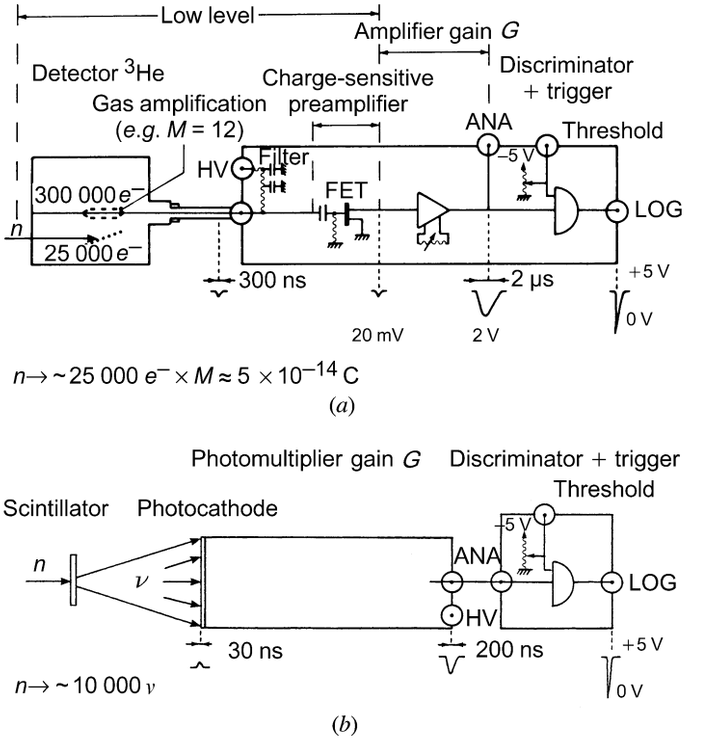

Fig. 7.3.4.1. Electronic chain following (*a*) an ^{3}He gas detector and (*b*) a scintillation detector.

a constant incident flux [see Fig. 7.3.4.2(*c*)]. On this curve, the width of the plateau and a value of the slope about 10^{-4} (in relative variation of counts per mV) give an indication of the detector quality. A good compromise is to set the threshold T at the middle of the plateau.

It is also necessary to verify that the detector high voltage, *i.e.* the gas-amplification coefficient M (see Subsection 7.3.3.1), is well adapted. With the value of the threshold T adjusted as above, the number of counts per unit time is plotted as a function of the high voltage [see Fig. 7.3.4.2(*d*)]. Typical values for the width of the plateau and its slope are 200 V and a few per cent per 100 V. If the high-voltage setting given by the manufacturer must be modified (owing to the worsening of the gas or constraints from the electronic chain, *etc.*), the complete adjustment procedure of the G and T parameters must be repeated.

The electronic adjustments and controls of types of detector other than $^{10}BF_3$ gas detectors are basically the same once the changes in the amplitude spectrum have been taken into account. We present in Fig. 7.3.4.2(*e*) the amplitude spectra for an ^{3}He gas detector with significant wall effects, for a ^{10}B solid-deposit detector with very low efficiency, and for a scintillator. The energy of the secondary particles produced in an ^{3}He gas detector is 765 keV, about three times less than in $^{10}BF_3$, reducing the signal-to-noise ratio; the relative importance of the wall effect is greater and extends to $A_0/4$. In the case of the ^{10}B deposit detector, only one of the secondary particles escapes the foil, so that we do not detect an amplitude A_0 corresponding to the full capture-reaction energy, but only that corresponding either to an average α or Li trace. The quality of the valleys depends on the t/r (foil thickness/particle range) ratio in the ^{10}B solid (see Fig. 7.3.3.2). The figure corresponds to a monitor where $t \ll r$. For the scintillator, the valley in the amplitude spectrum is not very good, even for good glasses and without γ radiation. The discrimination is therefore always much inferior to that of a gas detector. Moreover, the gain of the photomultiplier is very sensitive to the high voltage and has long-term stability problems.

7.3.5. Typical detection systems

7.3.5.1. *Single detectors*

In order to measure the scattered intensities, the single detector is mounted in a shield equipped with a collimator between sample and detector. The collimator is adapted to the sample (5 to 20′ Soller collimator for a powder diffractometer, or a hole adapted to the size of the beam diffracted by a single crystal). The sensitive area of the detector matches the size of the collimated diffracted beam. This geometry allows one to localize the scattered beam with adequate resolution and to avoid parasitic neutrons. In a powder diffraction measurement, the detector is scanned with a goniometer, each step being monitored.

7.3.5.2. *Position-sensitive detectors*

With the advantages of speed and simultaneity of data collection over broad angular ranges, position-sensitive detectors

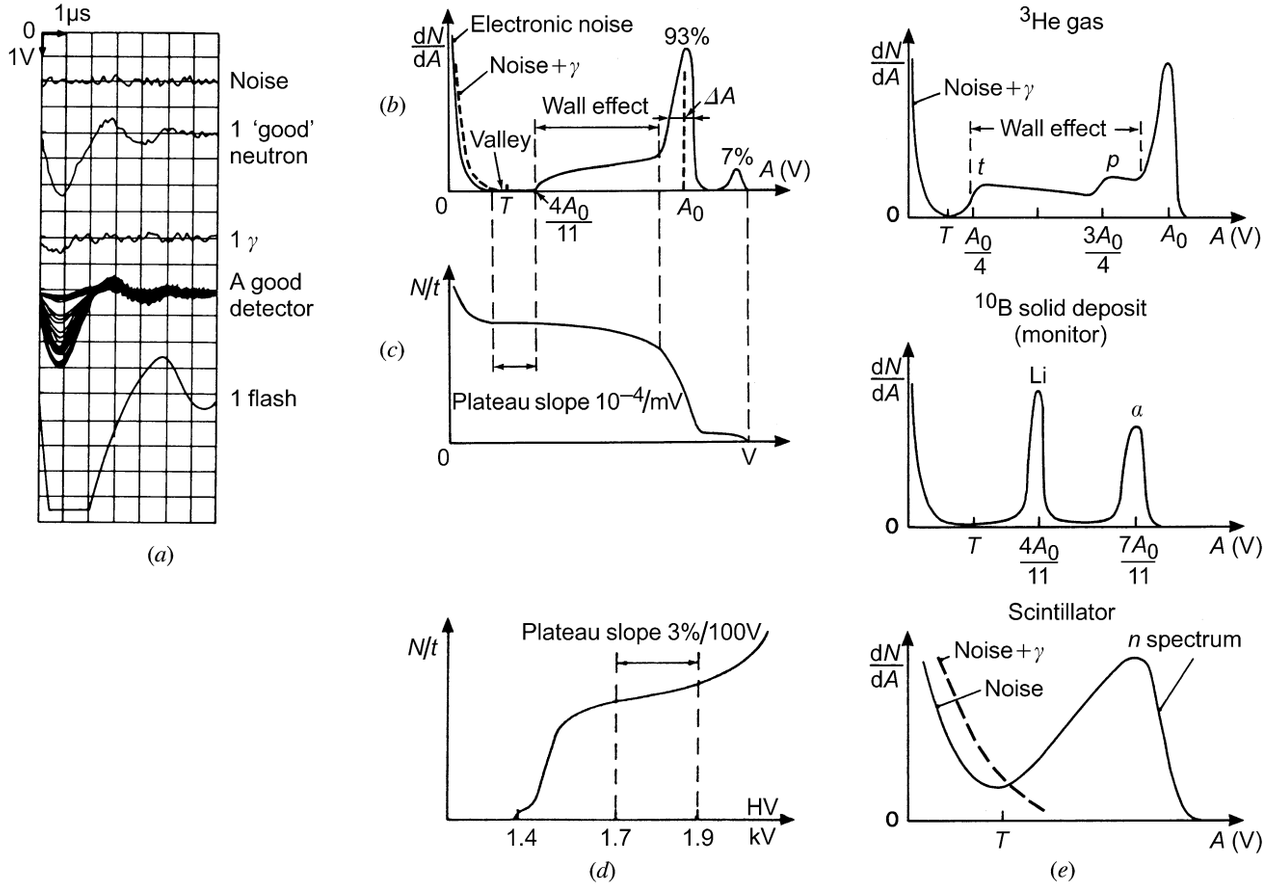

Fig. 7.3.4.2. (*a*) Characteristic $^{10}BF_3$ gas-detector analogue pulses seen on an oscilloscope. (*b*) $^{10}BF_3$ amplitude spectrum. (*c*) Plateau of a $^{10}BF_3$ detector as a function of the threshold voltage. (*d*) Typical plateau of a $^{10}BF_3$ detector in proportional mode as a function of the high voltage. (*e*) Amplitude spectra of various detectors.

(PSDs) have seen considerable development (Convert & Chieux, 1986). They are based on the fundamental detection processes described in Section 7.3.3. Their dimensions, the introduction of various systems for position encoding and decoding, and the multiplication of the number of detection chains (with necessary adjustments and controls) have produced detection systems of a complexity that can no longer be grasped by a researcher only occasionally involved in neutron-scattering experiments. The following lines give only a very crude introduction to PSDs at a descriptive level.

A PSD is always mounted in a shield that has an opening limited by the cone defined by the sample size and the detection area. Given the large opening in the shield, the PSD is very sensitive to parasitic neutrons, especially those coming from materials in the main monochromatic beam. However, if sufficient care is taken with the sample environment and beam-stop design, the signal-to-noise ratio may be as good as or even better than in a single detector. The scattering angle is determined by the angular position of the origin of the PSD, the sample-to-detector distance, and the location of the neutron capture in the PSD.

In a PSD, each individual neutron-capture reaction in the continuous converter is localized *via* an internal encoding system followed by electronic decoding. There are three types of PSD: the gas resistive wire, the gas multielectrode, and the Anger camera (scintillation).

(*a*) *Gas PSD with resistance encoding*. The simplest examples of this type of PSD are one-dimensional detectors in which the neutron-converter gas is contained in a cylindrical stainless-steel tube with a central, fine resistive wire anode. The amplitudes of the output pulses from charge-sensitive amplifiers attached to each end of the anode are then compared to derive the positional coordinate of the neutron. An alternative method of deriving the positional information is RC (resistance capacitance) encoding followed by time decoding (Borkowski & Kopp, 1975). Two-dimensional RC encoding PSDs have been developed. One of the solutions is to have a group of wires interconnected by a chain of resistors with amplifiers at the resistor chain nodes (Boie, Fischer, Inagaki, Merritt, Okuno & Radeka, 1982).

(*b*) *Gas multi-electrode PSD*. The simplest examples of this type of PSD are one-dimensional detectors with a small number of discrete electrodes, *e.g.* 64 parallel anode wires separated by 2.54 mm. Each anode wire has an amplifier. A logic system analyses the amplitudes of the output pulses corresponding to one neutron that are collected by one, two, or three neighbouring wires, and decides on which wire the neutron was detected. Large curved one-dimensional PSDs have been built on this principle, *e.g.* 800 wires covering 80°. Two-dimensional PSDs based on the same principle use a matrix system in which a neutron gives rise to two sets of signals on two orthogonal systems of electrodes (Allemand, Bourdel, Roudaut, Convert, Ibel, Jacobé, Cotton & Farnoux, 1975).

(*c*) *Neutron Anger camera*. The principle of the Anger camera is to detect an incident photon or particle with a continuous area of scintillator. The light produced is allowed to disperse before entering an array of photomultipliers (PMs) whose analogue output signals are used to derive the position of the incident neutron. In one dimension, the localization is achieved by a row of PMs (Naday & Schaefer, 1983). In two-dimensional PSDs, a close-packed array of PMs allows the location of the scintillation to be determined by calculating the X and Y centroids using a resistor-weighting scheme (Strauss, Brenner, Lynch & Morgan, 1981).

Table 7.3.5.1 gives the characteristics of some PSDs, each example being a good compromise of detector characteristics adapted to the instrument needs, powder diffraction, single-crystal diffraction, and small-angle neutron scattering (SANS). From this table, it seems that the characteristics of the various types of PSD that have been presented are nearly equivalent. The homogeneity of neutron detection over the PSD sensitive area is better than 5% in all cases. Among those PSDs, the gas PSDs, which have been installed since the early 1970s, are the most commonly used. The definite advantage of the gas multi-electrode PSD is to digitize the encoding, thus offering very good stability and reliability of the neutron localization. The resistance-encoding gas PSD has less complex electronics and permits a choice of pixel size (elementary detection area) and thereby definition. The Anger camera also offers the same flexibility in the choice of the pixel size and, because of the small thickness of the scintillator (1–2 mm), has very little parallax and is well adapted to TOF measurements. However, the γ sensitivity of the scintillators is much higher than that of the gas PSDs.

PSDs permit a simultaneous measurement of intensities over relatively large areas. As compared with the scanned single detector, this opens the way to two possibilities, either shorter counting time (*e.g.* real-time experiments) or improved statistical precision. However, the high counting rates achieved, as well as the complexity of the detection, increase the effective dead time and the occurrence of defects. The efficient use of a PSD therefore requires a detailed understanding of its operation (detection process, encoding–decoding, data storage, *etc.*) and periodic tests and calibrations.

7.3.5.3. *Banks of detectors*

When it is useful to have a large detection area without requiring spatial continuity of the detection, the solution is in the juxtaposition of several detectors. The selection of the type of detectors, the way of regrouping them, and the design of the collimation system depend on the measuring instrument. An appropriate geometry will optimize the signal-to-noise ratio and the instrumental resolution.

Banks of single detectors, up to 64 covering up to 160° in the diffraction plane with Soller collimators in front of each detector, are used for powder diffractometers in reactors [D1A and D2B, Institut Laue–Langevin (1988)]. The relative position of the detectors plus collimators and their response to the neutron intensity have to be measured and calibrated. The bank of detectors is scanned in small steps over the interval between two successive detectors in order to obtain a complete diagram over the angular range of the bank.

In a similar way, a juxtaposition of small PSDs with individual collimators is also used [D4, Institut Laue–Langevin (1988)].

In the case of spallation sources, the time-of-flight powder diffractometers are made of arrays of detectors at selected diffraction angles, to increase the detection area (Isis, 1992). Whenever it is possible, the time focusing geometry is used (Windsor, 1981). This implies a particular alignment of the detector array in order for it to become equivalent to one detector at one angle.

On the same instrument [HRPD, SANDALS, LAD (Isis, 1992)], various types of detector are used (^{3}He gas single detectors of small diameter, Li glass or Li+ZnS scintillators). For each selected diffraction angle, the choice of detector depends on the required resolution, which is better for scintillators because of their small thickness, and on other properties of the detectors (background, stability, γ discrimination), which are better for ^{3}He detectors.

Table 7.3.5.1. *Characteristics of some PSDs*

1D = one dimensional; 2D = two dimensional; *F*/ = flat; *C*/ = 1D curved; *X* = single crystal.

	Gas Resistance encoding		Gas Multi-electrode		Scintillation Anger camera	
	1D	2D	1D	2D	1D	2D
Location	*F*/ MURR (USA)	*F*/ ORNL (USA)	*F*/ ILL (France) *C*/ CENG (France)	*F*/ ILL (France) *C*/ ILL (France)	*F*/ Jülich (FRG)	*F*/ ANL (USA)
Instrument reference	Powder (1)	SANS (2)	*F*/ Liquids (3) *C*/ Powder (4)	*F*/ SANS (3,5) *C*/ *X* (3)	Powder (6)	*X* (7)
Detection area (mm)	$l = 610$ ($Ø = 25.4$)	650×650	*F*/ $l = 162.5$ ($h = 70$) *C*/ $l = 2096$ or 80° ($h = 70$)	*F*/ 640×640 *C*/ 1300×80 or $64° \times 4°$	$l = 744$ ($h = 20$)	300×300
Cell size or pixel (mm)		10×10	*F*/ 2.54 *C*/ 2.62 or 0.1°	*F*/ 5×5 *C*/ 2.54×5	0.7	0.3×0.3
Resolution (mm)	2.5	10×10	*F*/ 3.2 *C*/ 2.6	*F*/ 5×5 *C*/ 3×6.6	2.5	2.7×2.7
Efficiency (%)	70 (1.3 Å)	90 (4.75 Å)	*F*/ 90 (0.7 Å) *C*/ 52 (2.5 Å)	*F*/ 75 (11 Å) *C*/ 85 (1.5 Å)	70 (1.2 Å)	80 (1.8 Å)

MURR: Missouri University Research Reactor, Columbia, Missouri, USA.
ORNL: Oak Ridge National Laboratory, Tennessee, USA.
ILL: Institut Laue–Langevin, Grenoble, France.
ANL: Argonne National Laboratory, Argonne, Illinois, USA.
CENG: Centre d'Etudes Nucléaires de Grenoble, Grenoble, France.

References: (1) Berliner, Mildner, Sudol & Taub (1983); (2) Abele, Allin, Clay, Fowler & Kopp (1981); (3) Institut Laue–Langevin (1988); (4) Roudaut (1983); (5) Ibel (1976); (6) Schaefer, Naday & Will (1983); (7) Strauss, Brenner, Chou, Schultz & Roche (1983).

7.3.6. Characteristics of detection systems

We shall present and comment on some characteristics of detectors plus electronic chains in operational conditions.

(*a*) *Intrinsic background* (*i.e.* with the reactor or neutron source shut down). The intrinsic background level is about 6 counts h^{-1} for an ^{3}He, 3 bar (1 bar = 10^5 Pa) detector (Ø 50 mm, *L* 100 mm) in operational conditions. Of course, it is very important to protect the low-level part of the amplifier from the discriminator and trigger by separating these two stages very carefully, and from electric and electronic parasites by using good ground connections. Additional parasitic effects might be produced by (i) high-voltage flashes in the detector or in dirty or deficient plugs, (ii) microphony, and (iii) particle emission by the detector walls (*e.g.* uranium impurities in aluminium, or activation).

(*b*) γ *discrimination*. The γ discrimination of an ^{3}He detector is said to be 10^{-8}. From our own experience, we can say that a pure ^{3}He detector is insensitive to a γ dose up to 10 mGy h^{-1} (1 rem h^{-1}). However, additional gases increase the γ-detection efficiency (Fischer, Radeka & Boie, 1983). For a good scintillator, the γ discrimination is of the order of 10^{-4} (Kurz & Schelten, 1983).

(*c*) *Stability*. Under good conditions, the gas-detector stability has been verified to be better than 3×10^{-4}/day and 10^{-3}/month. The stability of operational scintillators is probably about 10^{-3}/day but it is known to drift over longer periods of time.

(*d*) *Dead time and non-linear effects due to the count rate*. The gas detector has a dead time of 1–10 μs depending on the duration of the analogue pulse, which is fixed by the detector plus adapted electronic chain. The scintillator has a dead time about 10 times shorter, *i.e.* 0.2 to 1 μs. A rule of thumb is to keep the total dead time to less than 10% of the counting time, which fixes the maximum counting rate. This limits the effects of non-linearity of the dead time as a function of the counting rate. Non-linear effects in gas detectors are complex and due to (i) the distortion of the electrostatic field near the anode by the space charge, (ii) the decrease of the high voltage at the anode produced at high counting rates by the increased ionic current passing through the high-impedance filter, and (iii) the possible shift of the zero level of the charge preamplifier.

(*e*) *TOF requirements*. In a TOF experiment, it is important to know exactly the time and place of each neutron capture. The thickness of the detector must be as small as possible in relation to the total flight path (scintillators are roughly 10 times thinner than gas detectors). The delay between the neutron capture and the logic pulse given by the amplifier gives an additional error. Again, the scintillator is about 10 times faster.

7.3.7. Corrections to the intensity measurements depending on the detection system

A good diffractometer on a reactor is supposed to give point by point for each solid-angle element $d\Omega$ an exact image of the scattered intensity. This is never perfectly achieved in practice and necessitates some corrections. In all cases, it is very important to be aware that additional background might be created when part of the shielding or of the collimator intersect the monochromatic neutron beam. We suppose for the following discussion that this effect has been corrected or avoided. The wavelength dependence of the detector response (which is needed for inelasticity corrections or TOF measurements) is generally computed from the theoretical detector law [see equation (7.3.2.1)]. At each measuring point, the collected intensity is renormalized by the integrated incident neutron flux, which is measured by the monitoring device.

In the case of TOF measurements on a spallation source, the measured intensity must also be renormalized by the wavelength spectrum of the source, obtained from the measurement of an isotropic scatterer such as vanadium.

7.3.7.1. *Single detector*

For up to 10% of dead time in the counting rate, the correction for the dead-time loss is generally considered as linear. If Δt is the electronic dead time for one neutron (1–10 μs for the gas detectors) and n the number of counts per second, the dead-time correction factor is $1/(1 - n\Delta t)$.

7.3.7.2. *Banks of detectors*

In the case of a bank of detectors used for a powder diffractometer in a reactor, one has to calibrate the relative positions of the detectors and their response to the neutron intensity by scanning the detectors through a Bragg pattern.

In the case of TOF measurements, the detector banks are installed at fixed angles. For each detector, the measured intensity depends on the detector type, size, and distance to the sample. The neutron and γ background depends moreover on the detection angle. After background corrections, the intensities measured by each detector bank are calibrated and matched using the overlaps between spectra.

7.3.7.3. *Position-sensitive detectors*

(*a*) *Calibration of the position*. For multi-electrode PSDs, the relative position of the electrodes is fixed and verified at the time of construction. In the case of other PSDs with analogue encoding, an angular calibration is made periodically with the help of a Bragg pattern, a thin neutron beam, or a cadmium mask moved across a diffuse beam incident on the PSD (Berliner, Mildner, Sudol & Taub, 1983).

(*b*) *Calibration of the PSD homogeneity*. The response function might be dependent on the position within the PSD and possibly on the intensities collected at other parts of the PSD. The homogeneity of response of a PSD, which is normally better than 5%, can be calibrated to a much higher accuracy, since the stability of the PSDs is generally very good (*e.g.* 0.1% or better for gas PSDs). In the case of a reactor, the classical method of calibration is the use of an isotropic scatterer such as vanadium. The calibration is made at angles that avoid the very small vanadium Bragg peaks (or with displacement of the PSD to several positions) and that keep a low and isotropic background. Calibration factors, sometimes called cell-efficiency coefficients α_i, are then obtained. Considering the lack of isotropy of the vanadium pattern, this method is limited to about 1% accuracy. For small PSDs, a precision of 0.1% or better is obtainable by scanning the whole PSD with a step equal to the cell spacing through any nearly isotropic pattern.

(*c*) *Particular effects due to high intensities*. The dead time of a PSD is complex. It depends on multiple parameters (the independent amplifiers and the encoding–decoding procedure). However, if there is a unique decoding logic for the whole PSD, and if this gives the highest contribution to the dead time, the ratios of the peak intensities are then conserved. In the case of strong Bragg peaks, the parasitic effect of scattering by the PSD entrance window (*e.g.* 10 mm aluminium for high-pressure gas PSDs) is detectable and can be corrected after calibration (using an intense and well localized thin beam).

7.1.7 (*cont.*)

Rossi, J. P. (1978). *Digital technique for reducing television noise*. *SMPTE J.* **87**, 134–140.

Rozgonyi, G. A., Haszlo, S. E. & Statile, J. L. (1970). *Instantaneous video display of X-ray topographic images with resolving capabilities better than 15*. *Appl. Phys. Lett.* **16**, 443–446.

Sato, F., Maruyama, H., Goto, K., Fujimoto, I., Shidara, K., Kawamura, T., Hirai, T., Sakai, H. & Chikawa, J. (1993). *Characteristics of a new high-sensitivity X-ray imaging tube for video topography*. *Jpn. J. Appl. Phys.* **32**, 2142–2146.

7.1.8

Amemiya, Y. (1995). *Imaging plates for use with synchrotron radiation*. *J. Synchrotron Rad.* **2**, 13–21.

Amemiya, Y., Kishimoto, S., Matsushita, T., Satow, Y. & Ando, M. (1989). *Imaging plate for time-resolved X-ray measurements*. *Rev. Sci. Instrum.* **60**, 1552–1556.

Amemiya, Y., Matsushita, T., Nakagawa, A., Satow, Y., Miyahara, J. & Chikawa, J. (1988). *Design and performance of an imaging plate system for X-ray diffraction study*. *Nucl. Instrum. Methods*, A**266**, 645–653.

Amemiya, Y. & Miyahara, J. (1988). *Imaging plate illuminates many fields*. *Nature (London)*, **336**, 89–90.

Amemiya, Y., Wakabayashi, K., Tanaka, H., Ueno, Y. & Miyahara, J. (1987). *Laster-stimulated luminescence used to measure X-ray diffraction of a contracting striated muscle*. *Science*, **237**, 164–168.

Ito, M. & Amemiya, Y. (1991). *X-ray energy dependence and uniformity of an imaging plate detector*. *Nucl. Instrum. Methods*, A**310**, 369–372.

Kato, H., Miyahara, J. & Takano, M. (1985). *New computed radiography using scanning laser stimulated luminescence*. *Neurosurg. Rev.* **8**, 53–62.

Miyahara, J., Takahashi, K., Amemiya, Y., Kamiya, K. & Satow, Y. (1986). *A new type of X-ray area detector utilizing laser stimulated luminescence*. *Nucl. Instrum. Methods*, A**246**, 572–578.

Sakabe, N. (1991). *X-ray diffraction data collection system for modern protein crystallography with a Weissenberg camera and an imaging plate using synchrotron radiation*. *Nucl. Instrum. Methods*, A**303**, 448–463.

Sonoda, M., Takano, M., Miyahara, J. & Kato, H. (1983). *Computed radiography utilizing scanning laser stimulated luminescence*. *Radiology*, **148**, 833–838.

7.2

Burge, R. E. & van Toorn, P. (1980). *Multiple images and image processing in STEM*. *Scanning Electron Microscopy/* 1980, Vol. 1, pp. 81–91. AMF O'Hare/Chicago: SEM Inc.

Chapman, J. N., Craven, A. J. & Scott, C. P. (1989). *Electron detection in the analytical electron microscope*. *Ultramicroscopy,* **28**, 108–117.

Chapman, J. N. & Morrison, G. R. (1984). *Detector systems for transmission electron microscopy*. *J. Microsc. Spectrosc. Electron.* **9**, 329–340.

Craven, A. J. & Buggy, T. W. (1984). *Correcting electron energy loss spectra for artefacts introduced by a serial data collection system*. *J. Microsc.* **136**, 227–239.

Daberkow, L., Herrmann, K.-H., Liu, L. & Rau, W. D. (1991). *Performance of electron image convertors with YAG single-crystal screen and CCD sensor*. *Ultramicroscopy*, **38**, 215–223.

Fan, G. Y. & Ellisman, M. H. (1993). *High-sensitivity lens-coupled slow-scan CCD camera for transmission electron microscopy*. *Ultramicroscopy*, **52**, 21–29.

Farnell, G. C. & Flint, R. B. (1975). *Photographic aspects of electron microscopy*. *Principles and techniques of electron microscopy*, Vol. 5, edited by M. A. Hayat, pp. 19–61. New York: Van Nostrand Rheinhold.

Garlick, G. F. J. (1966). *Cathodo- and radioluminescence*. *Luminescence of inorganic solids*, edited by P. Goldberg, Chap. 12. London: Academic Press.

Guetter, E. & Menzel, M. (1978). *An external photographic system for electron microscopes*. *Electron microscopy 1978*, Vol. 1, edited by J. M. Sturgess, pp. 92–93. Toronto: Microscopical Society of Canada.

Hamilton, J. F. & Marchant, J. C. J. (1967). *Image recording in electron microscopy*. *J. Opt. Soc. Am.* **57**, 232–239.

Herrmann, K.-H. (1984). *Detection systems*. *Quantitative electron microscopy*, edited by J. N. Chapman & A. J. Craven, Chap. 4. Edinburgh University Press.

Herrmann, K.-H. & Krahl, D. (1984). *Electronic image recording in conventional electron microscopy*. *Advances in optical and electron microscopy*, edited by R. Barer & V. E. Cosslett, Chap. 1. London: Academic Press.

Ishizuka, K. (1993). *Analysis of electron image detection efficiency of slow-scan CCD cameras*. *Ultramicroscopy*, **52**, 7–20.

Isoda, S., Saitoh, K., Moriguchi, S. & Kobayashi, T. (1991). *Utility test of image plate as a high-resolution image-recording material for radiation-sensitive specimens*. *Ultramicroscopy*, **35**, 329–338.

Krivanek, O. L., Ahn, C. C. & Keeney, R. B. (1987). *Parallel detection electron spectrometer using quadrupole lenses*. *Ultramicroscopy*, **22**, 103–115.

Kujawa, S. & Krahl, D. (1992). *Performance of a low-noise CCD camera adapted to a transmission electron microscope*. *Ultramicroscopy*, **46**, 395–403.

Mori, N., Katoh, T., Oikawa, T., Miyahara, J. & Harada, Y. (1986). *Electron microscopy 1986*, Vol. 1, edited by T. Imura, S. Maruse & T. Suzuki, pp. 29–32. Tokyo: Japanese Society of Electron Microscopy.

Mori, N., Oikawa, T., Katoh, T., Miyahara, J. & Harada, Y. (1988). *Application of the ''imaging plate'' to TEM image recording*. *Ultramicroscopy*, **25**, 195–202.

Reimer, L. (1984). *Transmission electron microscopy*, Chap. 4.6. Berlin: Springer-Verlag.

Schauer, P. & Autrata, R. (1979). *Electro-optical properties of a scintillation detector in SEM*. *J. Microsc. Spectrosc. Electron.* **4**, 633–650.

Valentine, R. C. (1966). *The response of photographic emulsions to electrons*. *Advances in optical and electron microscopy*, edited by R. Barer & V. E. Cosslett, Chap. 5. London: Academic Press.

Zeitler, E. (1992). *The photographic emulsion as analog recorder of electrons*. *Ultramicroscopy*, **46**, 405–416.

7.3

Abele, R. K., Allin, G. W., Clay, W. T., Fowler, C. E. & Kopp, M. K. (1981). *Large-area proportional counter camera for the U.S. National Small-Angle Neutron Scattering Facility*. *IEEE Trans. Nucl. Sci.* **28**(1), 811–815.

7.3 (*cont.*)

Allemand, R., Bourdel, J., Roudaut, E., Convert, P., Ibel, K., Jacobé, J., Cotton, J. P. & Farnoux, B. (1975). *Position-sensitive detectors (P.S.D.) for neutron diffraction*. *Nucl. Instrum. Methods*, **126**, 29–42.

Baruchel, J., Malgrange, C. & Schlenker, M. (1983). *Neutron diffraction topography: using position-sensitive photographic detection to investigate defects and domains in single crystals*. *Position-sensitive detection of thermal neutrons,* edited by P. Convert & J. B. Forsyth, pp. 400–406. London: Academic Press.

Berliner, R., Mildner, D. F. R., Sudol, J. & Taub, H. (1983). *Position-sensitive detectors and data collection systems at the University of Missouri Research Reactor Facility*. *Position-sensitive detection of thermal neutrons*, edited by P. Convert & J. B. Forsyth, pp. 120–128. London: Academic Press.

Boie, R. A., Fischer, J., Inagaki, Y., Merritt, F. C., Okuno, H. & Radeka, V. (1982). *Two-dimensional high precision thermal neutron detector*. *Nucl. Instrum. Methods*, **200**, 533–545.

Borkowski, C. J. & Kopp, M. K. (1975). *Design and properties of position-sensitive proportional counters using resistance-capacitance position encoding*. *Rev. Sci. Instrum.* **46**, 951–962.

Convert, P. & Chieux, P. (1986). *From BF_3 counter to PSD. An impressive and continuous increase of the data acquisition rate*. *Fifty years of neutron diffraction,* edited by G. E. Bacon, pp. 218–227. Bristol: Adam Hilger.

Convert, P. & Forsyth, J. B. (1983). *Position-sensitive detection of thermal neutrons:* Part 1, *Introduction*. *Position-sensitive detection of thermal neutrons*, pp. 1–90. London: Academic Press.

Fischer, J., Radeka, V. & Boie, R. A. (1983). *High position resolution and accuracy in ^3He two-dimensional thermal neutron PSDs*. *Position-sensitive detection of thermal neutrons*, edited by P. Convert & J. B. Forsyth, pp. 129–140. London: Academic Press.

Hohlwein, D. (1983). *Photographic methods in neutron scattering*. *Position-sensitive detection of thermal neutrons*, edited by P. Convert & J. B. Forsyth, pp. 379–390. London: Academic Press.

Ibel, K. (1976). *The neutron small-angle camera D11 at the high-flux reactor, Grenoble*. *J. Appl. Cryst.* **9**, 296–309.

Institut Laue–Langevin (1988). *Guide to neutron research facilities at the ILL*. Grenoble: Institut Laue–Langevin.

Isis (1992). *User Guide*. Didcot: Rutherford Appleton Laboratory.

Kurz, R. & Schelten, J. (1983). *Properties of various scintillators for thermal neutron detection*. *Position-sensitive detection of thermal neutrons,* edited by P. Convert & J. B. Forsyth, pp. 192–196. London: Academic Press.

Naday, I. & Schaefer, W. (1983). *A new processing method and gain stabilisation for scintillation position-sensitive detectors*. *Position-sensitive detection of thermal neutrons,* edited by P. Convert & J. B. Forsyth, pp. 197–202. London: Academic Press.

Roudaut, E. (1983). *Evolution of position-sensitive detectors for neutron diffraction experiments from 1966 to 1982 in the Nuclear Centre of Grenoble*. *Position-sensitive detection of thermal neutrons,* edited by P. Convert & J. B. Forsyth, pp. 294–301. London: Academic Press.

Schaefer, W., Naday, I. & Will, G. (1983). *Neutron powder diffractometry with the linear position-sensitive scintillation detector*. *Position-sensitive detection of thermal neutrons*, edited by P. Convert & J. B. Forsyth, pp. 209–214. London: Academic Press.

Strauss, M. G., Brenner, R., Chou, H. P., Schultz, A. J. & Roche, C. T. (1983). *Spatial resolution of neutron position scintillation detectors*. *Position-sensitive detection of thermal neutrons,* edited by P. Convert & J. B. Forsyth, pp. 175–187. London: Academic Press.

Strauss, M. G., Brenner, R., Lynch, F. J. & Morgan, C. B. (1981). *2-D position-sensitive scintillation detector for neutrons*. *IEEE Trans. Nucl. Sci.* **28**(1), 800–806.

Thomas, P. (1972). *Production of sensitive converter screens for thermal neutron diffraction patterns*. *J. Appl. Cryst.* **5**, 373–374.

Whaling, W. (1958). *The energy loss of charged particles in matter*. *Handbuch der Physik,* Vol. 34. *Corpuscles and radiation in matter II*, edited by S. Flugge, pp. 193–217. Berlin: Springer-Verlag.

Windsor, C. G. (1981). *Pulsed neutron scattering*. London: Taylor and Francis.

Wolf, R. S. (1974). *Measurement of the gas constants for various proportional counter gas mixtures*. *Nucl. Instrum. Methods*, **115**, 461–463.

7.4.2

Bachmann, R., Kohler, H., Schulz, H. & Weber, H. (1985). *Structure investigation of a CaF_2-crystal with synchrotron radiation*. *Acta Cryst.* A**41**, 35–40.

Cooper, M. J. (1971). *The evaluation of thermal diffuse scattering of neutrons for a one velocity model*. *Acta Cryst.* A**27**, 148–157.

Dorner, B., Burkel, E., Illini, Th. & Peisl, J. (1987). *First measurement of a phonon dispersion curve by inelastic X-ray scattering*. *Z. Phys. B*, **69**, 179–183.

Helmholdt, R. B., Braam, A. W. M. & Vos, A. (1983). *Improved corrections for thermal diffuse scattering*. *Acta Cryst.* A**39**, 90–94.

Helmholdt, R. B. & Vos, A. (1977). *Errors in atomic parameters and electron density distributions due to thermal diffuse scattering of X-rays*. *Acta Cryst.* A**33**, 38–45.

International Tables for Crystallography (1992). Vol. B. *Reciprocal space*, edited by U. Shmueli. Dordrecht: Kluwer.

Jahn, H. A. (1942). *Diffuse scattering of X-rays by crystals*. *The Faxen–Waller theory and the surfaces of isodiffusion for cubic crystals*. *Proc R. Soc. London Ser. A*, **179**, 320–340; **180**, 476–483.

James, R. W. (1962). *The optical principles of the diffraction of X-rays*. London: Bell.

Krec, K. & Steiner, W. (1984). *Investigation of a silicon single crystal by means of the diffraction of Mössbauer radiation*. *Acta Cryst.* A**40**, 459–465.

Krec, K., Steiner, W., Pongratz, P. & Skalicky, P. (1984). *Separation of elastically and inelastically scattered γ-radiation by Mössbauer diffraction*. *Acta Cryst.* A**40**, 465–468.

Merisalo, M. & Kurittu, J. (1978). *Correction of integrated Bragg intensities for anisotropic thermal scattering*. *J. Appl. Cryst.* **11**, 179–183.

Popa, N. C. & Willis, B. T. M. (1994). *Thermal diffuse scattering in time-of-flight diffractometry*. *Acta Cryst.* A**50**, 57–63.